วารสารวิชาการ วิศวกรรมศาสตร์ ม.อบ.
UBU Engineering Journal

บทความวิจัย

Simulation model for controlling of the photovoltaic water pumping system

Rati Wongsathan

Department of Electrical Engineering, Faculty of Engineering and Technology, North-Chiang Mai University, 169 Hang Dong, Chiang Mai 50230, Thailand

E-mail: rati@northcm.ac.th, rati1003@gmail.com; Telephone: 0 5381 9999; Fax. 0 5381 9998

Received 15 November 2019; Revised 10 December 2019; Accepted 20 January 2020

Abstract

The work aims to model a standalone photovoltaic-powered water pumping system (PVWPS) and implements the converter-controller based upon the maximum power point tracking (MPPT) technique. The MPPT-based fuzzy logic controllers with the Mamdani inference method using the triangular and Gaussian membership functions in the design are applied to improve the performance of the PVWPS. The parameters, including fuzzy rules of the MPPT-MFLC, are designed and adjusted by the expert. In the test, a 1 kW-PV generator and the centrifugal pump direct-driven by the permanent magnet DC motor, as load, interfaced with the buck converter are demonstrated through the simulations under weather variations at a constant head pumping. As a result, the proposed controllers provide 7.4% – 8% more energy utilization efficiency against the conventional tracking Perturb and Observe algorithm. Furthermore, they can increase the PV efficiency of up to 10%, and consequently, the overall system efficiency is maximized, including water discharge.

Keywords

photovoltaic water pumping system; fuzzy logic-based controller; maximum power point tracking; energy utilization efficiency

1. Introduction

Photovoltaic (PV) systems are necessary for many powered applications, especially in the remote area where the electricity is unavailable. The PV-powered water pumping system (PVWPS) is regarded among the most promising PV power applications and is a significant tool in supplying water to such the area. The optimal design of this system can result in effective long-term cost-saving, whereas the appropriate power control algorithm can increase the PV energy utilization efficiency, and consequently maximize the overall PVWPS efficiency [1]. Various PVWPS models have been presented in the literature [2-7]. The modeling of PVWPSs with a brushless DC motor (BLDCM), a permanent magnet DC motor (PMDCM), and a single-phase induction motor (SPIM) is proposed in [2], [3], and [4], respectively. By the comparison, the PMDC motor outperforms the SPIM in terms of providing high performance and simple to use without requiring an inverter and field excitation [4]. Besides, the PVWPSs using a permanent-magnet synchronous motor [5] and a switched reluctance motor [6] are modeled and simulated using the Matlab/Simulink software.

Mathematical model derivation of the PVWPS which is composed of a PV array and a centrifugal pump driven by a PMDCM without the interfaced controller-converter has been simulated in the previous work [7]. As a result, the operating points of the PV generator deviate away from the maximum power points (MPPs), and consequently, the performance of the PVWPS in terms of the energy utilization efficiency is degraded by 23% – 96%, especially under poor weather conditions. To continue the work, the main aim is to overcome

such a problem using the controller-converter for shifting the operating point toward the MPP.

However, the generated PV power output is nonlinearly weather-dependent. As such, the MPP for the given weather conditions could not be tracked easily. Integrating the converter and controller utilized the maximum power point tracking (MPPT) technique can help to detect the MPPs effectively. Till now, various MPPT-algorithms have been used to control the power in the PV systems. They are generally divided into two main groups: conventional- and artificial intelligence (AI)-based schemes. The Perturb and Observe (P&O) [8] and incremental conductance (IC) [9] methods among the conventional methods are widely used because of the simplicity in implementation, but they are inefficient under rapidly changing weathers. Alternatively, AI-based controllers, such as neural network controller (NNC) [10], fuzzy logic controller (FLC) [10], neuro-fuzzy controller (NFC) [11], have been used to address such problem.

In this paper, a mathematical derivation of the PVWPS is presented prior to design the MPPT-controller. The FLCs based on the Mamdani fuzzy inference system (M-FIS) due to more interpretable and understandable in design fuzzy output than the Sugeno-FIS with two types of membership function (MF) in the design: triangular MF (TMF) and Gaussian MF (GMF), which are denoted by MFLC-TMF and MFLC-GMF, respectively. They generate the duty ratio to control the switching buck converter interfaced between PV generator and motor-pump. The system parameters of the MFLCs (the parameters of TMFs and GMFs, and fuzzy rules) are designed and adjusted by the expert. The proposed MPPT-MFLCs are applied to the PVWPS and carried out under weather variations. The transient and steady-state responses, including the PV energy utilization efficiency, of the proposed controllers, are compared with those of the P&O method. The PVWPS model and MPPT-controllers design are implemented using Matlab software, and the system performances are analyzed through the simulated results.

In the following, Section 2 describes a mathematical model of the PVWPS. The design of the MPPT-MFLCs is detailed in Section 3. The results are discussed in Section 4. Finally, Section 5 summarizes the conclusion.

2. The description of the PVWPS

A schematic diagram of the PVWPS-controller is shown in Fig. 1 which is composed of a 1 kW-PV array as the current source, a DC-DC buck converter, the MPPT-controllers in regulating the PV voltage or power output, and the electric-powered pump of a centrifugal pump-type driven by the PMDC motor, as a load.

To simulate the PV current-voltage (I_{PV}-V_{PV}) characteristics, the PV array composed of N_s and N_p connected in series and parallel, respectively, is modeled using a single diode model [12] which is described using 5-parameter: the photo generated current I_{ph}, reverse diode saturation current I_{sd}, cell series resistance R_s, cell shunts resistance R_{sh}, and the solar ideal factor of the diode n. The relationship between I_{PV} and V_{PV} is given implicitly with those parameters as

$$I_{PV} = N_P I_{ph} - N_P I_{sd}\left[\exp\frac{qV_{temp}}{nK_BT} - 1\right] - \left[\frac{V_{temp}}{R_{sh}/N_P}\right], \quad (1)$$

where $V_{temp} = V_{PV}/N_S + I_{PV}R_S/N_P$, q is the electron charge (1.6×10^{-19} C), T is absolute temperature (K), and $K_B \approx 1.38\times10^{-23}$ J/K (Boltzmann's constant). The parameter I_{ph} is given by,

$$I_{ph} = \left[I_{sc} + K_I(T - T_0)\right]\times\left(\frac{G}{G_0}\right), \quad (2)$$

where G is the solar irradiance (W/m^2), I_{sc} is the short circuit current under the standard test conditions (STC) of T_0 = 298 K and G_0 = 1000

W/m^2, and K_I is cells short-circuit current temperature coefficient. The parameter I_{sd} depended on the temperature is given by,

$$I_{sd} = I_{sd,0}\left[\frac{T}{T_0}\right]^3 \exp\left[\frac{qE_g}{nk_B}\left(\frac{1}{T_0}-\frac{1}{T}\right)\right], \qquad (3)$$

where $I_{sd,0}$ is the saturation current at STC, E_g is the energy gap of the semiconductor (eV).

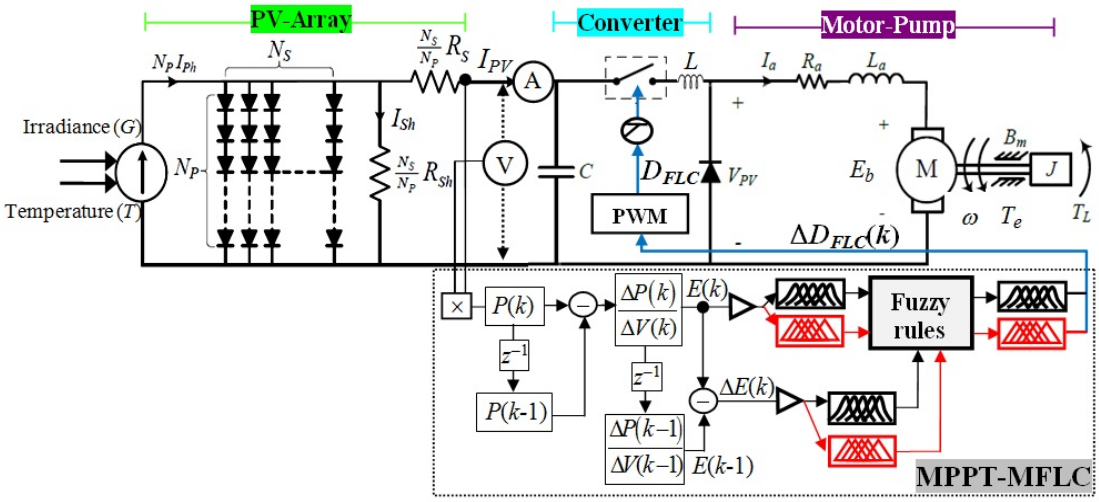

Figure 1 A schematic diagram of the PVWPS with the proposed MPPT-MFLCs

In this work, a commercial polycrystalline silicon module (rated power 130 W, open-circuit voltage 22 V, short-circuit current 8 A, and voltage and current at the MPP of 17.4 and 7.5, respectively) is employed as the case study, see Table 1 for further information. The average water requirement is 20 m^3/day for an available 6-hour day estimation, then the flow rate (Q) for the pump, on average, is 3.3 m^3/h and is varied in the range 0.5 – 5.0 m^3/h. The total dynamic head (TDH) is assumed to be 20 m. The PV power output converted to the hydraulic power (P_h) is varied in the range 100 – 1,000 W. According to the specifications of the motor-pump used in the PVPWS (Table 1) and the requirement of the outputs mentioned earlier, the PV modules are wired in series to increase voltage for driving the utilized PMDC motor. Then, N_S is sufficiently selected as 8 (≈1000 W/130 W).

Under the STC, the PV parameters are obtained as I_{ph} = 8 A, I_s = 8.8 μA, R_s = 0.016 Ω, R_{sh} = 690 Ω, and n = 1.877 through the method as referred to [13]. For providing the information to the MPPT-controller design, the preliminary results of I_{PV}-V_{PV}, Eq. (1), and PV power (P_{PV})-V_{PV} characteristics under the weather conditions are depicted in Fig. 2(a) and (b), respectively. It is seen that the maximum PV powers cover the desired specification range.

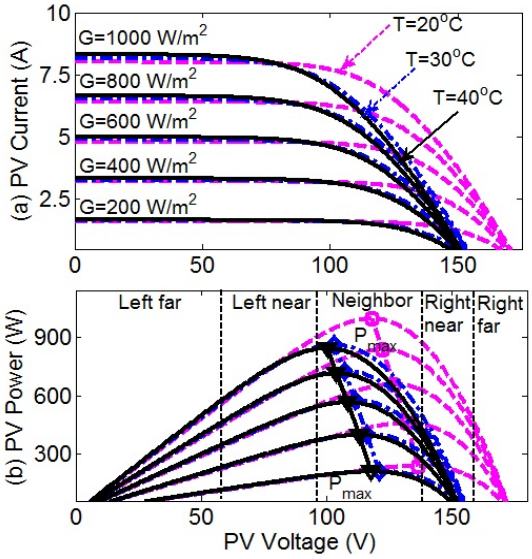

Figure 2 (a) I_{PV}-V_{PV}, and (b) P_{PV}-V_{PV} characteristics of the utilized PV array with the partitioned regions for FLC design

The PV efficiency (η_{PV}) can be expressed as

$$\eta_{PV} = \frac{P_{PV}}{G \times S_{PV}} \times 100 , \quad (4)$$

where S_{PV} is the effective surface area (for the utilized PV array, S_{PV} = (1.50×0.7)×8 m^2).

To minimize the system, a PMDC motor without a separate field power supply and having a low starting torque that easily matches with the PV array characteristics is employed and coupled with a pump. For a constant flux, the dynamic equation of the PMDC motor is given by [14],

$$V_a = I_a R_a + L_a \frac{dI_a}{dt} + E_b , \quad (5)$$

where E_b=$K_e\omega$ is the induced back electromotive force voltage (emf), K_e is motor voltage constant, ω is the angular velocity and V_a, I_a, R_a and L_a is the armature voltage, current, resistance and winding inductance, respectively. The torque balance of the PMDC motor is expressed as,

$$T_e = K_t I_a = J \frac{d\omega}{dt} + B\omega + C + T_L , \quad (6)$$

where T_e is electromagnetic torque, T_L is load torque, K_t is the motor torque constant, B is the viscous friction constant, J is the rotational inertia and C is the torque constant for rotational losses.

At the steady state, i.e., dI_a/dt=0 and $d\omega/dt$=0, from Eq. (6), the power generated from the PV array $P_{PV}(G, T)$ and transferred to the motor under the given G and T conditions is given by,

$$P_{PV}(G,T) = I_a^2 R_a + I_a E_b . \quad (7)$$

By solving I_a from Eq. (6), when T_e=E_bI_a/ω, and subsequently placing into Eq. (7), then

$$P_{PV}(G,T) = \frac{Ra}{K_t^2}\left(B^2\omega^2 + 2B\omega(C+T_L) + (C+T_L)^2\right) + B\omega^2 + (C+T_L)\omega. \quad (8)$$

The centrifugal pump widely used in PVWPS is considered in this work because of the design simplicity, high efficiency, and broad range of flow rates and heads. Moreover, it has long operated period, even for low irradiance, and well matching to the maximum power locus of the PV generator [15]. Herein, the driving torque of the centrifugal pump is as follows:

$$T_L = A_L + K_L \omega^l , \quad (9)$$

where A_L is the load friction, and K_L and l=1.8 are the constant parameters of the pump. By assuming that C and A_L are equal to zero, and substituting Eq. (9) into Eq. (8), then

$$P_{PV}(G,T) = \left(\frac{K_L^2 R_a}{K_t^2}\right)\omega^{3.6} + \left(\frac{2BK_L R_a}{K_t^2} + K_L\right)\omega^{2.8} + \left(\frac{B^2 R_a}{K_t^2} + B\right)\omega^2 . \quad (10)$$

The matching between the PV array and PMDC motor in case of without the controller/converter interface is illustrated in Fig. 3. It is seen that the operating points (the intersection between the PV array and motor load characteristics as red dots) deviate away from the MPPs (black dots), especially under low irradiance. In addition, the motor would not start working unless the irradiance reaches 200 W/m^2. Therefore, the motor may operate in the locked rotor condition causing heat instead mechanical output that shortens the motor's life. To handle this problem, the device called a linear current booster (LCB) is applied at the beginning in the early morning with very low irradiance. However, after the motor starts to run even the irradiance lower than 200 W/m^2 is sufficient to drive the motor.

From Fig. 3, to step down the PV voltage to a rated motor or load matching, the buck converter is employed by regulating the switching duty cycle (D) according to the pulse width modulation (PWM) signal generated from the MPPT-controller. The parameters required in designing the buck converter are listed in Table 1.

Table 1 The specifications of the motor-pump

Specification	Value
PV module: Polycrystalline silicon commercial	
- Type and model	SHARP, ND-130T1J
- Module efficiency	13.1%
- Maximum operating voltage	600 V
- Ambient temperature	-40°C to +90°C
- Fuse rating	15 A
DC-DC Buck converter	
- Ripple current and voltage	5%
- Switching frequency	200 kHz
- Input-output voltage	200 and 120 V
- Minimum inductance	250 μH
- Minimum capacitance	20 μF
PMDC motor	
- Maximum voltage (V_a)	120 V
- Maximum current (I_a)	9.2 A
- Maximum speed (ω)	157 rad/s
- Armature resistance (R_a)	1.5 Ω
- Armature inductance (L_a)	0.2 H
- Voltage constant (K_t)	0.676V/rad/sec
- Torque constant (K_L)	0.676 Nm/A
- Motor friction (A_m)	0.2 Nm
Centrifugal pump	
- Rotational inertia (J)	0.0236 Kg m^2
- Viscous friction coefficient (B)	0.00238 Nm/(rad/sec)
- Load torque constant (K_e)	0.00039 Nm/(rad/sec)
- Load friction (A_L)	0.3 Nm

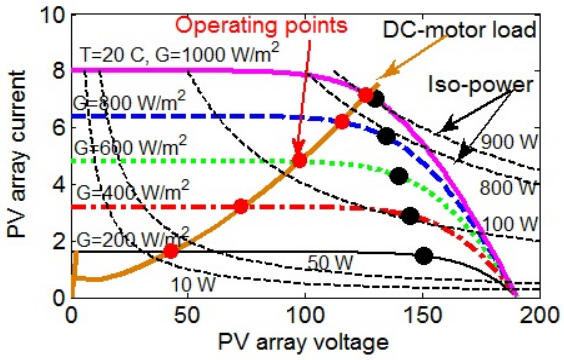

Figure 3 The I_{PV}-V_{PV} array with the MPPs against motor-pump load characteristic and the operating points

3. MPPT-controller design

In this section, two types of MMPT-controllers (MFLC-TMF and MFLC-GMF) are described in detail of the design. There are typically 3 steps of FIS including fuzzification, inference rule, and defuzzification. From the MFLC scheme (Fig. 1), the electrical variables measured from the PV array, I_{PV} and V_{PV}, are used to determined the fuzzy inputs, $E(k)$ and $\Delta E(k)$, at the k^{th} sampling time as

$$E(k)=\frac{\Delta P(k)}{\Delta V(k)}=\frac{P(k)-P(k-1)}{V(k)-V(k-1)}, \quad (11)$$

And

$$\Delta E(k)=E(k)-E(k-1), \quad (12)$$

respectively, whereas the increment duty ratio (ΔD) is the output. The slope of P_{PV}-V_{PV} curve or $E(k)$ is utilized to determine the magnitude of ΔD for preventing fluctuations, whereas $\Delta E(k)$ provides the sign of ΔD to control the movement direction of the operating point towards the MPP.

From Fig. 2(b), the crisp input of $E(k)$ can be characterized using 5 different fuzzy subsets based on the span of 5 MFs: *NB* (negative big), *PB* (positive big), *NS* (negative small), *PS* (positive small) and *Z* (zero), corresponding to 5 regions of the P_{PV}-V_{PV} curve: left- and right-far from MPP, left- and right-near to MPP, and a neighbor of MPP, respectively. *PB* and *PS* indicate that the operating points located on the left-hand side (LHS) of MPP

which are far from and nearby the MPP, respectively. Whereas, *NB* and *NS* indicate that the operating points located on the right-hand side (RHS) of MPP which are far from and nearby the MPP, respectively. Lastly, *Z* indicates that the operating point locates very near around the MPP. Similarly, the crisp input $\Delta E(k)$ is also partitioned into 5 different subsets as, {*NB*, *NS*, *Z*, *PS*, and *PB*}. The MFs are characterized by the TMFs and GMFs.

In the fuzzification, the given crisp of fuzzy inputs are fuzzified to the degree of TMFs and GMFs, $\mu \in [0, 1]$, by

$$\mu_{TMF}(x) = \max\left(\min\left(\frac{x-p}{q-p}, \frac{r-x}{r-q}\right), 0\right), \qquad (13)$$

and

$$\mu_{GMF}(x) = \exp\left[-\left(\frac{x-c}{\sigma}\right)^2\right], \qquad (14)$$

respectively, where x is the value of crisp input; p's, q's, and r's are the triangular parameters; and c's and σ's are the parameters of center and width of the Gaussian function, respectively.

In the inference rule, the combination of the inputs E and ΔE generates the total of 25 subsets (rules) in the fuzzy output universe. The Mamdani outputs of all rules are calculated and combined to obtain the fuzzy output. In M-FIS rules, the input-output relation of the j^{th}-rule at sampling time k+1 is of the following form. **IF** $E(k)$ is *PB* and $\Delta E(k)$ is *NB* **THEN** $\Delta D_{MFLC,j}(k+1)$ is *PB*.

Through the rule inference of using max-min operation, the output of the j^{th} rule is as, $\mu(\Delta D_{MFLC,j})=\max(\min\{\mu(E),\mu(\Delta E)\})$, where $\mu(E)$, $\mu(\Delta E)$ and $\mu(\Delta D_{MFLC})$ are the degree of MFs of E, ΔE and $\Delta D_{MFLC,j}$, respectively. Lastly, on the defuzzification step, the crisp output (ΔD_{MFLC}) is determined by defuzzyfying the fuzzy output using the centre of gravity (COG) technique as,

$$\Delta D_{MFLC} = \frac{\sum_{j=1}^{25} \Delta D_{MFLC,j}\,\mu(\Delta D_{MFLC,j})}{\sum_{j=1}^{25} \mu(\Delta D_{MFLC,j})}. \qquad (15)$$

In this work, to build up the MPPT-MFLCs, the parameters of the TMFs and GMFs are trial-and-error tuned which are depicted in Fig. 4 and Fig. 5, respectively. Whereas, the understandable 25-fuzzy-rule in Table 2 have been designed by the expert. The designing principle of the 25-fuzzy rule in determining the relationship between fuzzy inputs (E and ΔE), and the fuzzy output (ΔD) is explained as follows.

In case the negative slope of the *P-V* curve or $E(k)$ is *NB*, when $\Delta E(k)$ is *Z* indicates that the operating point is placed on right near the MPP, Fig. 2 (b), then the duty ratio, $D(k+1)=D(k)+\Delta D(k)$, would be increased so that the input impedance increases and the operating point moves as close as possible to the MPP at the LHS. Therefore, $\Delta D(k)$ is suppressed and set as *PS* to prevent from missing the MPP and oscillations. When $\Delta E(k)$ is *NB* or *NS* which means the trajectory of the operating point towards the RHS, then the output $\Delta D(k)$ is set as *PS* or *PB* for increasing the duty ratio. The operating point moves from RHS to LHS along the *P-V* curve. On the other hand, when $\Delta E(k)$ is *PS* or *PB* means the direction towards the LHS then $\Delta D(k)$ would be set as *Z*. In case $E(k)$ is *NS*, when $\Delta E(k)$ is either negative (*NS* and *NB*) or Z or positive (*PS* and *PB*), $\Delta D(k)$ is set similarly.

In case $E(k)$ is *PB* and $\Delta E(k)$ is *Z* that represents the operating point is placed on left near the MPP, Fig. 2 (b), then the duty ratio would be decreased so that the input impedance increases and the operating point moves to the MPP on the RHS. Therefore, $\Delta D(k)$ is suppressed and set as *NS* to prevent from missing the MPP. When $\Delta E(k)$ is *NB* or *NS*, then $\Delta D(k)$ would be set as *Z*. When $\Delta E(k)$ is *PB* or *PS*, the duty ratio would be set to decrease. Then, $\Delta D(k)$ would use *NB* or *NS*, respectively. In case $E(k)$ is *PS*, when $\Delta E(k)$ is either negative or zero or positive the $\Delta D(k)$ is set similarly.

In case $E(k)$ is Z and $\Delta E(k)$ is Z indicates that the MPP is found, $\Delta D(k)$ would be set as Z. When $\Delta E(k)$ is NB or NS, $\Delta D(k)$ would be set as PB or PS, respectively. When $\Delta E(k)$ is PS or PB, $\Delta D(k)$ would be set as NB or NS, respectively.

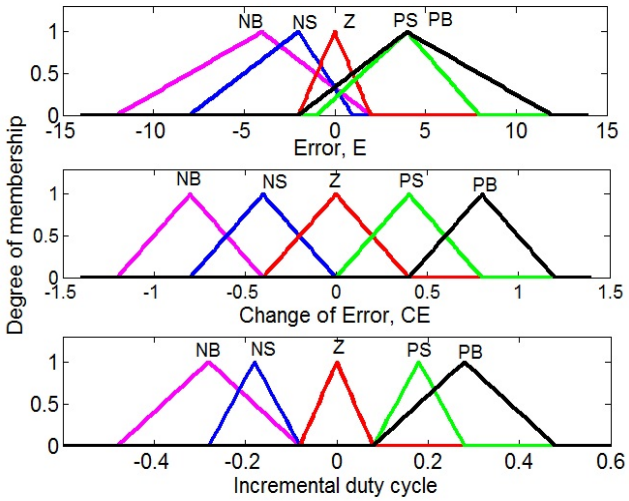

Figure 4 The shapes of the TMFs tuned by the expert

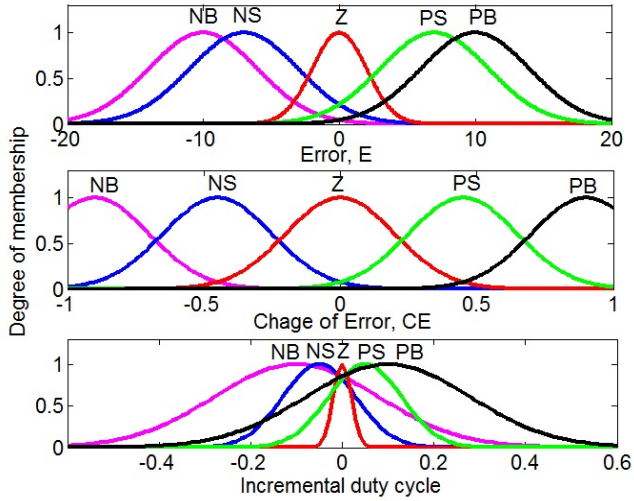

Figure 5 The shapes of the GMFs tuned by the expert

Table 2 Fuzzy inference rules designed by the expert

ΔE \ E	*NB*	*NS*	*Z*	*PS*	*PB*
NB	*PS*	*PS*	*PB*	*Z*	*Z*
NS	*PB*	*PS*	*PS*	*Z*	*Z*
Z	*PS*	*Z*	*Z*	*Z*	*NS*
PS	*Z*	*Z*	*NS*	*NS*	*NB*
PB	*Z*	*Z*	*NB*	*NS*	*NS*

It is seen that the shapes of TMFs and GMFs of ΔD are not evenly distributed along the UOD, but they are more dense in the range of -0.2 – 0.2 which is a sensitive work zone. The controller needs a small value of ΔD to achieve the MPP.

4. Results and discussion

For the MFLCs design, the UODs are identified as: $E \in [-20, 20]$, $\Delta E \in [-20, 20]$, and $\Delta D \in [-0.5, 0.5]$. The controlled results of the MPPT-P&O method with a fixed-step size of duty ratio (0.05) and the MFLCs are depicted in Fig. 7 under the setup of 7 different G and T conditions varying between 400 – 1000 W/m^2 and 20 – 40°C, respectively (Fig. 6). The cases show the good matching between I_{PV}, V_{PV}, ω and D with their optimal values under weather variations. For the transient and steady-state response of the power control (Fig. 8), the P&O able to provide fast response time but more oscillations that cause energy waste and heat. On the other hand, the proposed MFLCs provide fast transient response without the overshoot, and reach near the MPP with negligible oscillations under all set up weather conditions.

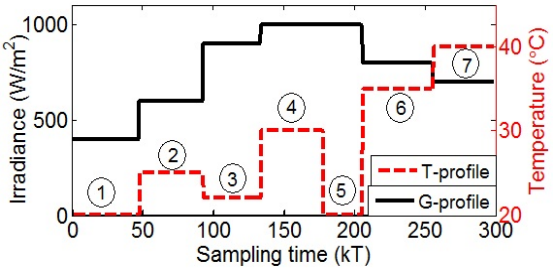

Figure 6 Setup weather conditions of G and

In comparison the energy efficiency among the controllers, the energy utilization efficiency over the time interval $[t_i, t_f]$ is used and defined as

$$\eta_{utilize} = \int_{t_i}^{t_f} \frac{P_{MPPT}(t)}{P_{MPP}(t)} dt \times 100 \ , \qquad (16)$$

where P_{MPPT} represents the PV power obtained from the MPPT-controllers and P_{MMP} is the PV power at the MPP.

Consider the tracking power shown in Fig. 8 in which the consequently numerical resulted in Table 3, the proposed MFLC-TMF, MFLC-GMF, and P&O method provide by about 85%, 83%, and 77%, averagely in energy utilization efficiency, respectively. The MFLC-GMF can generate the total tracking power slightly higher than that from the MFLC-TMF, but has the cost of computing the power tracking control and the difficulty in implementing with the microcontroller due to the nonlinear mapping of the Gaussian function.

T

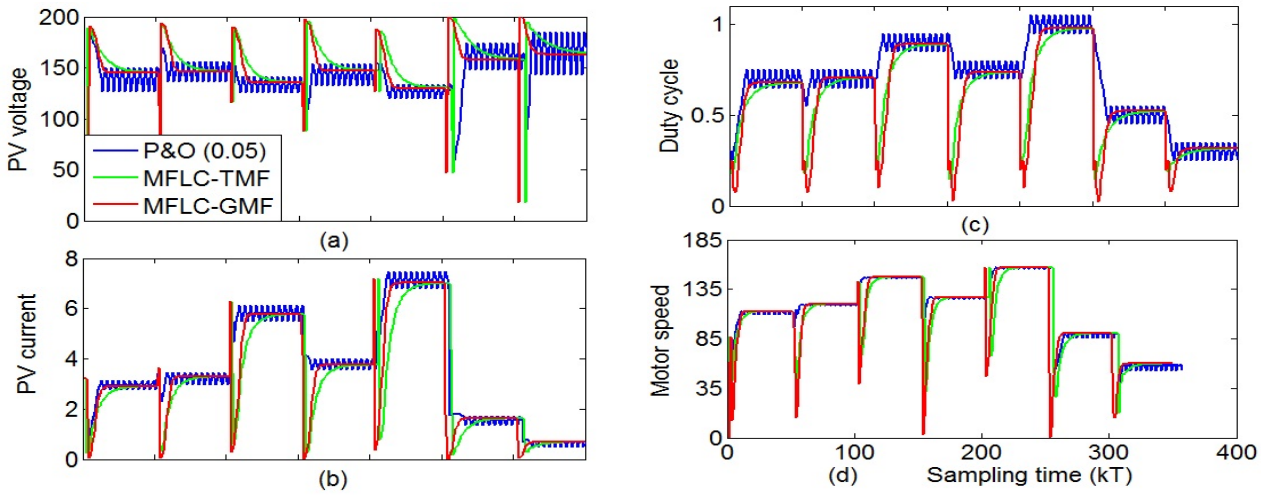

Figure 7 Control results of the MFLC-TMF, MFLC-GMF, and P&O method

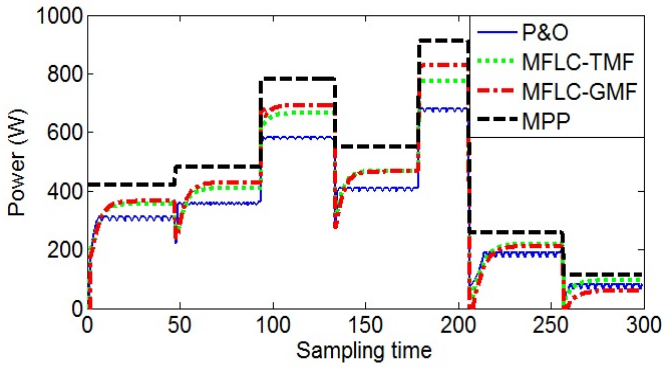

Figure 8 Comparison of the tracking power between the MFLC-TMF, MFLC-GMF, and P&O method

Table 3 Performances of the PVWPS/MPPT-MFLCs

Weather conditions			P_{MMP}	MFLC-TMF					MFLC-GMF				
No.	G (W/m^2)	T (°C)	(W)	P_{MMPT} (W)	η_{PV} Eq. (4)	$\eta_{utilize}$ Eq. (16)	ω (rad/s)	Q (l/s)	P_{MMPT} (W)	η_{PV} Eq. (4)	$\eta_{utilize}$ Eq. (16)	ω (rad/s)	Q (l/s)
1	400	20	420	357	10.63	85.0	112.8	1.51	365	10.86	86.9	115.4	1.55
2	600	25	481.8	410	8.13	85.1	113.1	2.16	427.5	8.48	88.7	117.9	2.26
3	900	22	782.4	665	8.80	91.3	138.6	3.32	691.5	9.15	94.9	144.1	3.46
4	1000	28	551.7	468.8	5.58	84.9	121.1	2.56	465.8	5.55	84.4	120.4	2.54
5	1000	20	911.8	775	9.23	85.0	128.9	4.04	828	9.86	90.8	137.7	4.31
6	800	35	257.8	218	3.24	84.5	89.8	1.14	210.9	3.14	81.8	86.9	1.10
7	700	40	113.6	96.2	1.64	84.7	65.7	0.45	60.2	1.02	53.0	41.1	0.28
average				**427.1**	**6.87%**	**85%**	**110**	**2.17**	**435.5**	**6.75%**	**83%**	**109**	**2.21**

From Table 3, the MPPT-FLCs present good performances under low-temperature, especially the 1st- and 5th-conditions even low irradiance in the 1st-condition. For very high temperature and low or medium irradiance, their performances are significantly degraded. Furthermore, the PV efficiency (η_{PV}) of the MFLC-TMF and MFLC-GMF varies in the range of 1.64% – 10.63% and 1.02% – 10.86%, respectively. The results of the P&O method are not shown here but its PV efficiency is lower than the MFLCs which is varied from 0.93% to 9.8%. Therefore, the motor speed and water discharge of the MFLCs are higher than the rest.

5. Conclusion

In this work, the MPPT-based MFLCs applied to the PVWPS are proposed. The fuzzy parameters, including the fuzzy rules, are derived by the expert. When the PVWPS-MFLCs are carried out under weather variations, the proposed MFLC-TMF outperforms the rest in terms of the energy utilization efficiency by 2% – 8%. In addition, the proposed MFLCs can increase the PV efficiency of up to 6.75% – 6.85%, and consequently, the motor speed, including water discharge, is maximized. However, due to the conventional FLC-design the optimal performance may not achieve, continuing this work, a stochastic optimization is adopted in tuning the controller parameters while minimizing the complexity.

Acknowledgment

This research was solely supported by the Research Institute of North-Chiang Mai University (NCU), Chiang Mai, Thailand.

References

[1] Abdourraziq S, Bachtiri RE. Optimum design of photovoltaic water pumping system application. *WASET*, 2016;10(6):767-773.

[2] Lawrance W, Wichert B, Langridge D. Simulation and performance of a photovoltaic pumping system. *Proceeding of the International Conference on Power Electronics and Drive System;* 1995 Feb. 21-24; Singapore: 1995.

[3] Minai AF, Tariq A, Alam Q. Theoretical and experimental analysis of photovoltaic water pumping system. *Proc. of the India International Conference on Power Electronics (IICPE'10)*. 2011 Jan. 28-30; New Delhi, India: 2011.

[4] Chandrasekaran N, Thyagarajah K. Simulation and experimental validation of AC motor and PMDC motor pumping system fed by photovoltaic cell. *Indian Journal of Engineering and Material Sciences*. 2014; 21(1):93-103.

[5] Dubey M, Sharma S, Saxena R. Solar PV stand-alone water pumping system employing PMSM drive. *Proc. of the IEEE Students' Conference*

on Electrical, Electron. And Computer Science (SCEECS'14). 2014; March 1-2; Bhopa, India: 2014.

[6] Belliwali S, Chakravarti A, Raju AB. Mathematical modeling and simulation of directly coupled PV water pumping system employing switched reluctance motor. *Proceeding of the IEEE PES Innovative Smart Grid Technologies—India (ISGT India'11)*; 2011; Dec. 1-3; Kollam, Kerala, India: 2011.

[7] Seedadan I, Wongsathan R. Nuangnit A. Modeling and simulation of a standalone PV solar-powered water pumping system. *Proceeding of the 41st Electrical Engineering Conference (EECon-41)*; 2018; Nov. 21-23; Ubonratchathani, Thailand: 2018.

[8] Harrag A, Titraoui A, Bahri H, Messalti S. Photovoltaic pumping system-comparative study analysis between direct and indirect coupling mode technologies and materials for renewable energy, environment and Sustainability. *AIP Conference Proceeding 2017*; 2017 Feb. 23;1814(1):1-8.

[9] Kumar B, Chauhan YK, Shrivastava V. Performance analysis of a water pumping system supplied by a photovoltaic generator with different maximum power point tracking techniques. *Songklanakarin Journal of Science and Technology*. 2014;36(1):107-113.

[10] Abu-Rub H, Iqbal A, Ahmed SKM, Peng FZ, Li Y, Baoming G. Quasi-Z-Source inverter-based photovoltaic generation system with maximum power tracking control using ANFIS. *IEEE Transaction on Sustainable Energy*. 2013;4(1):11-20.

[11] Priyadarshi N, Padmanaban S, Mihet-Popa L, Blaabjerg F, Azam F. Maximum power point tracking for brushless DC motor driven photovoltaic pumping system using hybrid ANFIS-FLOWER pollination optimization algorithm. *Energies.* 2018;11(5):1-15.

[12] Muhsen DH, Haider HT, Shahadi HI. Parameter extraction of single-diode PV-module model using electromagnetism-like algorithm. *Journal of Engineering and Sustainable Development*. 2018; 22(2):161-172.

[13] Wongsathan R, Seedadan I. Artificial intelligence and ANFIS reduced rule for equivalent parameter estimation of PV module on various weather conditions utilized for MPPT. *International Journal of Renewable Energy* 2017;12(1):38-55.

[14] Krishnan R. *Electric motor drives: modeling, analysis, and control. vol. 626*, Prentice Hall Upper Saddle Rive, NJ, 2001.

[15] Al-Waeli AHA *et al*. Optimum design and evaluation of solar water pumping system for rural areas. *International Journal of Renewable Energy Research*. 2017;7(1):12-21.